

Operando Unveiling of Hydrogen Spillover Mechanisms on Tungsten Oxide Surfaces

Haoyi Li, Mona Abdelgaid, Jay R. Paudel, Noah P. Holzapfel, Veronica Augustyn, James R. McKone, Giannis Mpourmpakis,* and Ethan J. Crumlin*



Cite This: *J. Am. Chem. Soc.* 2025, 147, 6472–6479



Read Online

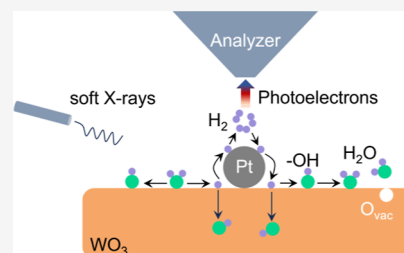
ACCESS |

Metrics & More

Article Recommendations

Supporting Information

ABSTRACT: Hydrogen spillover is an important process in catalytic hydrogenation reactions, facilitating H_2 activation and modulating surface chemistry of reducible oxide catalysts. This study focuses on the *operando* unveiling of platinum-induced hydrogen spillover on monoclinic tungsten trioxide ($\gamma\text{-WO}_3$), employing ambient pressure X-ray photoelectron spectroscopy, density functional theory calculations and microkinetic modeling to investigate the dynamic evolution of surface states at varied temperatures. At room temperature, hydrogen spillover results in the formation of W^{5+} and hydrogen intermediates (hydroxyl species and adsorbed water), facilitated by Pt metal clusters. With increasing temperature, water desorption, reverse hydrogen spillover and surface-to-bulk diffusion of hydrogen atoms compete with each other, leading initially to reoxidation and then further reduction of W atoms in the near-surface. The combined experimental results and simulations provide a comprehensive understanding of the mechanisms underlying hydrogen interaction with reducible metal oxides, lending insights of relevance to the design of enhanced hydrogenation catalysts.



INTRODUCTION

Hydrogen (H_2) plays a crucial role in the chemical industry for global decarbonization, particularly in catalytic hydrogenation and hydrogen evolution reactions.^{1–4} Generally, for hydrogenation reactions taking place on solid surfaces, H_2 first undergoes dissociative adsorption to yield surface-bound hydrogen species, H^* (thermochemical equivalent of H^+/e^-). These act as the foundation for subsequent reaction steps. Hence, the thermochemistry and dynamics of H^* formation and further reactions are understood to have a major effect on catalytic performance.^{5,6} This means it is vitally important to explore the chemical reactivity of solid–gas interfaces in reducing environments to obtain insights into the design of enhanced hydrogenation catalysts.

On the surfaces of catalysts containing transition metal oxides, which are commonly used as solid supports and active hydrogenation catalysts, H_2 molecules usually need to overcome a considerable activation energy barrier to adsorb and dissociate.^{7,8} To accelerate this elementary reaction step at low temperatures (lower than 500 °C),^{7,9} noble metal nanoparticles, such as platinum (Pt), are often introduced to the oxide surface to catalyze H_2 dissociation. In this process, homolytic dissociative chemisorption of H_2 molecules first occurs on Pt metal surfaces, followed by the transfer of Pt-bound H^* species to proximal metal oxides, forming hydrogen intermediates, i.e., hydroxyl species ($-\text{OH}$) and adsorbed water (H_2O_{ads}) along with concomitant reduction of the metal element in the oxide.^{8,10,11} This process is referred to as

hydrogen spillover, which serves as a key mechanism of pivotal H_2 -involved transformations of energy conversion.^{12–15}

Studies to date have shown that reducible metal oxides, such as tungsten trioxide (WO_3), are especially effective substrates for hydrogen spillover via proton-coupled electron transfer (PCET).^{16–18} However, the fundamental mechanisms of PCET in reducible metal oxides are still the subject of considerable debate.^{8,19,20} This is in part due to the difficulty of distinguishing between redox chemistry on the surface versus bulk sites for hydrogen bonding in oxides like WO_3 that can undergo bulk hydrogenation to form hydrogen bronzes (e.g., $H_x\text{WO}_3$). The wide range of surface structures and terminations offers multiple pathways for (I) hydrogen insertion into the bulk oxide lattice (H_{bulk});^{18,21} (II) the formation of H_2 molecules by reverse hydrogen spillover;^{22,23} or (III) the accumulation of oxygen vacancies (O_{vac}) via H_2O_{ads} desorption.^{12,15,20} Distinguishing the formation of H_{bulk} , H_2 molecules, and O_{vac} is challenging but important for manipulating hydrogen reactivity, especially through *operando* techniques at elevated temperatures.

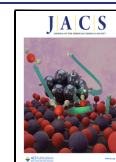
In spite of extensive prior studies on hydrogen spillover, relatively little work has been done regarding dynamic

Received: October 1, 2024

Revised: January 6, 2025

Accepted: January 7, 2025

Published: January 18, 2025



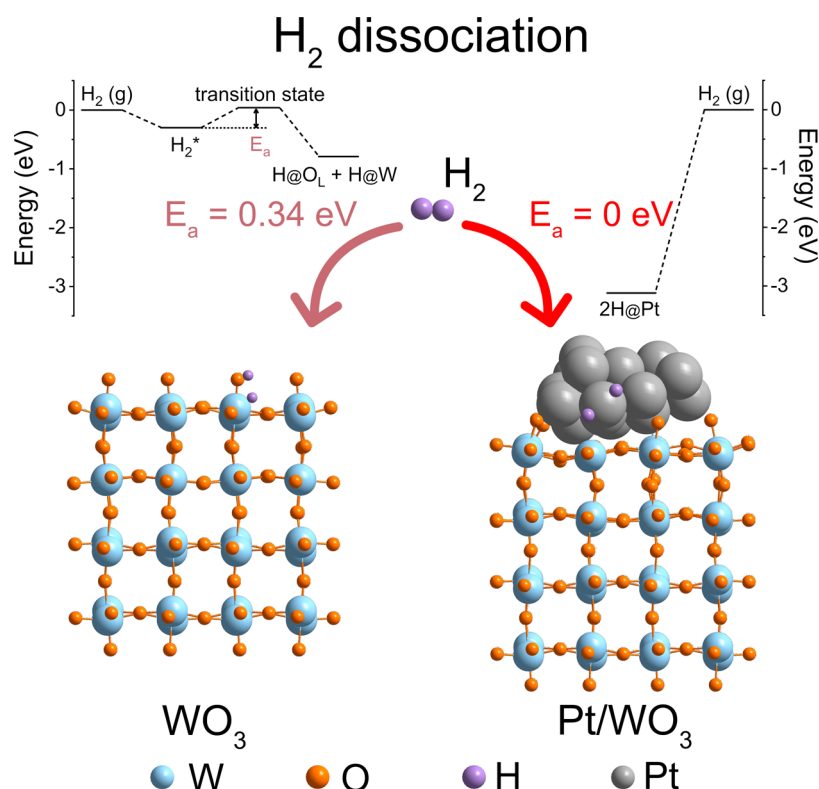


Figure 1. Schematic H_2 dissociation on the monoclinic WO_3 (001) surface with and without Pt metal clusters with corresponding electronic energy profiles. Comparison of the E_a highlights the kinetically favorable H_2 dissociation on Pt/ WO_3 .

spectroscopic visualization under real-world catalytic conditions.^{12,24–27} This is important because it facilitates the understanding of reaction mechanisms particularly when compared with theoretical predictions. In this work, we focused on Pt-decorated monoclinic $\gamma\text{-WO}_3$ as the prototypical platform for hydrogen spillover.^{17,21,28} Density functional theory (DFT) calculations indicate the spontaneous homolytic dissociation of H_2 on Pt metal and subsequent facile transfer of hydrogen atoms to WO_3 , favoring the formation of hydrogen intermediates at room temperature and O_{vac} at elevated temperature on the surface of WO_3 . Using synchrotron radiation-based ambient pressure X-ray photoelectron spectroscopy (APXPS) with soft X-rays, we investigated the interactions between H_2 and WO_3 thin films over a range of temperatures with and without Pt metal clusters. Upon exposure to H_2 , bare WO_3 exhibits unaltered features up to at least 400 °C, which agrees with extensive prior work invoking spillover mechanisms that require H_2 activation and dissociation at a secondary catalytic site.^{8,10,11} With the addition of Pt metal (Pt/ WO_3), we observed the dynamic evolution of W and O species via *operando* time- and temperature-dependent APXPS strategies for the first time. Using the simulation of electron spectra for surface analysis (SESSA) software, we concreted the surface components of the WO_3 at different conditions, which inform the chemical dynamics on the surface of Pt/ WO_3 in the temperature-dependent APXPS experiments. These results demonstrate that the fundamental mechanisms of Pt-induced hydrogen spillover entail at least three reactive processes—H-binding, O_{vac} formation, and H-migration via reverse hydrogen spillover and surface-to-bulk diffusion—each of which contributes significantly to the observed W redox chemistry over the temperature range from 25 to 400 °C.

RESULTS AND DISCUSSION

We constructed two models to study H_2 adsorption and dissociation on monoclinic WO_3 through DFT calculations (Figure 1): WO_3 with Pt metal clusters at the surface (Pt/ WO_3) and bare WO_3 (WO_3). We first examined the interaction of molecular H_2 with the pristine WO_3 (001) surface. The molecular adsorption of H_2 on bare WO_3 is weak, with a binding energy of -0.30 eV and H–H bond length of 0.76 Å. Next, heterolytic dissociation of molecular H_2 takes place on the terminal W–O site pairs with an exothermic binding energy of -0.79 eV. However, this reaction step is kinetically hindered with an activation barrier height (E_a) of 0.34 eV. In contrast, homolytic dissociation of H_2 over Pt metal clusters is highly exothermic (binding energy = -3.12 eV) with $E_a = 0$ eV, consistent with previous reports.^{11,25,29–31} These computational findings show that Pt metal clusters significantly facilitate H_2 activation and dissociation under conditions in which the same behaviors of H_2 are kinetically inhibited on the WO_3 surfaces.

Based on these theoretical calculations, we prepared two types of samples, Pt/ WO_3 and WO_3 , respectively (Figures S1–S3), using a reported method.^{18,21,32–35} We adopted the well-established method to create a standard catalyst platform—Pt metal clusters on monoclinic WO_3 to *operando* investigate Pt-induced hydrogen spillover mechanisms on monoclinic WO_3 , rather than developing a novel material system or intentionally targeting specific Pt lattice facets. We then used synchrotron radiation-based APXPS with soft X-rays to understand interactions between H_2 and monoclinic WO_3 at room temperature (Figure 2a). WO_3 was first introduced to the APXPS system and treated with 200 mTorr of oxygen (O_2) at 400 °C for 30 min to remove carbon contaminations (Figure

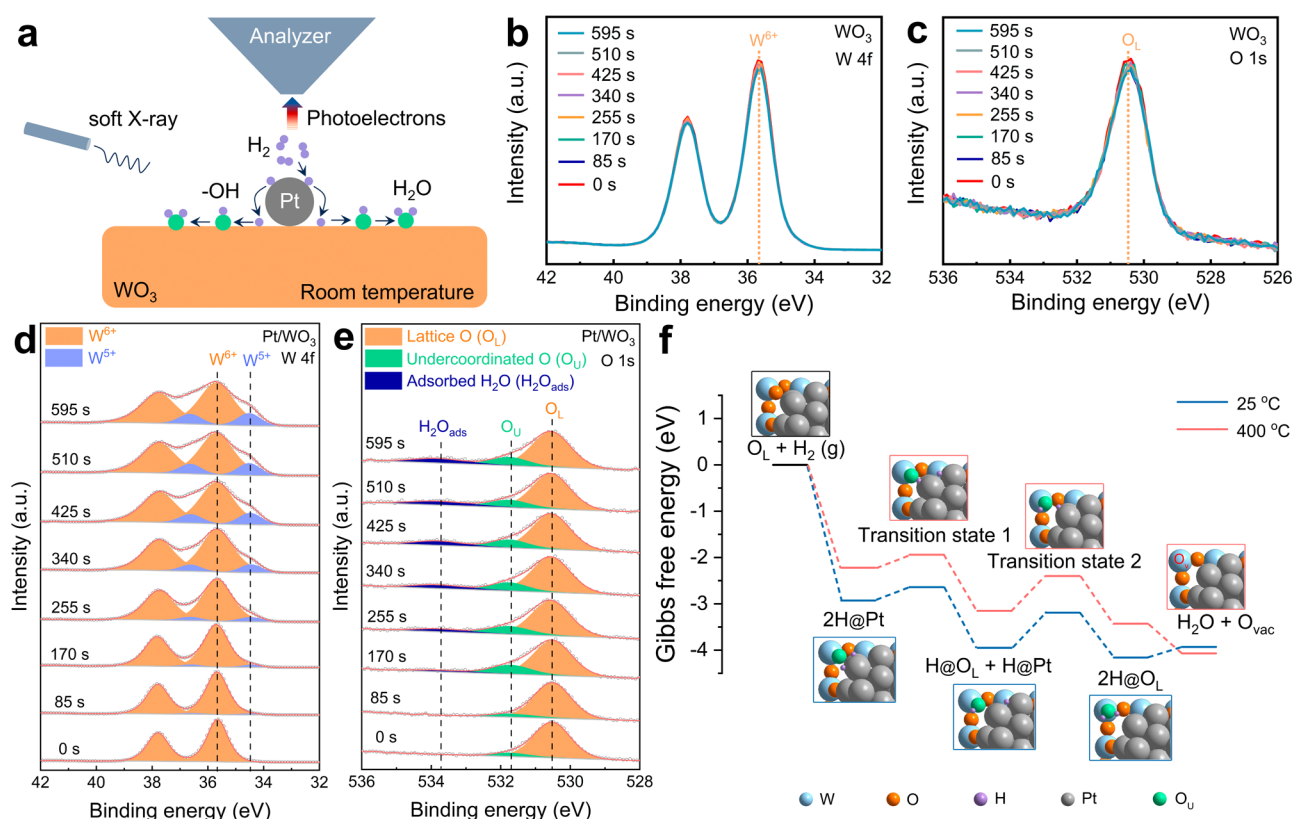


Figure 2. Operando monitoring of hydrogen spillover on WO_3 surfaces at room temperature using APXPS with soft X-rays. (a) Schematic representation of the experimental configuration and reaction steps associated with hydrogen spillover on Pt/ WO_3 using APXPS with soft X-rays; solid green, purple, and gray circles represent O, H, and Pt elements, respectively. (b,c) W 4f and O 1s regions of XPS spectra (PE = 570 eV) on bare WO_3 collected at room temperature under 5 mTorr of H_2 gas. (d,e) W 4f and O 1s regions of Pt/ WO_3 under the same conditions as panels (b,c). (f) Gibbs free energy profiles of elementary steps for H-dissociation and O_{vac} formation on Pt/ WO_3 at different temperatures from DFT calculations with corresponding local structures for each step.

S2). After O_2 treatment, the W 4f and O 1s XPS spectra were measured at room temperature with a photon energy (PE) of 570 eV. Analysis of the spectra showed the presence of W^{6+} and preponderant lattice oxygen (O_{L}), respectively, consistent with fully oxidized WO_3 (Figure S4). We then changed the gas environment to 5 mTorr of H_2 , followed by consecutive collections of W 4f and O 1s regions to monitor compositional changes at the solid–gas interfaces (PE = 570 eV). As depicted in Figure 2b,c, the spectra remained constant, suggesting no interactions between H_2 molecules and bare WO_3 (Figure S5), and also excluding any beam-induced effects on the sample. These results align with our DFT calculations, indicating H_2 dissociation and spillover are kinetically inhibited at room temperature on bare WO_3 .

We further performed analogous APXPS measurements on Pt/ WO_3 , where Pt metal clusters were *in situ* deposited on the bare WO_3 surface in the APXPS chamber via evaporation (Figure S3).^{33–35} Initial surface composition with respect to W and O signals were indistinguishable from those of bare WO_3 (Figure S4), suggesting the minimal interaction between Pt metal clusters and the WO_3 substrate. However, upon 5 mTorr of H_2 , clear signs of hydrogen spillover were observed based on the presence of W^{5+} (Figure 2d), along with the formation of $\text{H}_2\text{O}_{\text{ads}}$ and an increased amount of undercoordinated oxygen (O_{U}) species (Figure 2e), which are reported signatures of PCET on the Pt/ WO_3 surface.^{8,12} This hydrogen spillover process reached equilibrium within 10 min (Figure S6 and Table S1). The stark contrast in H_2 interaction with Pt/ WO_3

and WO_3 reveals the critical role of Pt metal in facilitating hydrogen dissociation and spillover, in agreement with prior work.^{8,10,11} Furthermore, after hydrogen spillover, Pt/ WO_3 can be fully restored through O_2 treatment (Figure S7) and displays consistent behavior during a subsequent hydrogen spillover cycle, demonstrating remarkable reversibility.

To aid in interpreting the spectroscopic results, DFT calculations were performed to estimate binding energies (BEs) for various O species on the WO_3 surfaces (Figure S8). The simulated peaks informed the assignments of the experimentally measured XPS peaks for O species. The peak located approximately 1.2 eV higher in BE than the O_{L} peak could be attributed to the oxygen in surface hydroxyl ($-\text{OH}$), chemisorbed H_2O , or near O_{vac} species formed upon water desorption.^{36–38} This feature has therefore been assigned as undercoordinated oxygen (O_{U}) in Figure 2e.

Mechanistically, hydrogen spillover entails dissociative chemisorption of molecular H_2 on the Pt metal cluster. Afterward, the Pt-bound H^* species migrate to surface terminal oxygen sites of WO_3 through surface diffusion or proton-coupled electron transfer.^{39,40} Further spillover results in the formation of surface bound water ($\text{H}_2\text{O}_{\text{ads}}$), and O_{vac} then forms through $\text{H}_2\text{O}_{\text{ads}}$ desorption to the gas phase. The Gibbs free energy (ΔG) profile for hydrogen spillover on Pt/ WO_3 at 25 and 400 °C are depicted in Figure 2f. In the first elementary step, H_2 molecules dissociate spontaneously on Pt metal clusters. Then, the first hydrogen atom migrates to the WO_3 (001) surface and forms $-\text{OH}$, which is thermodynamically

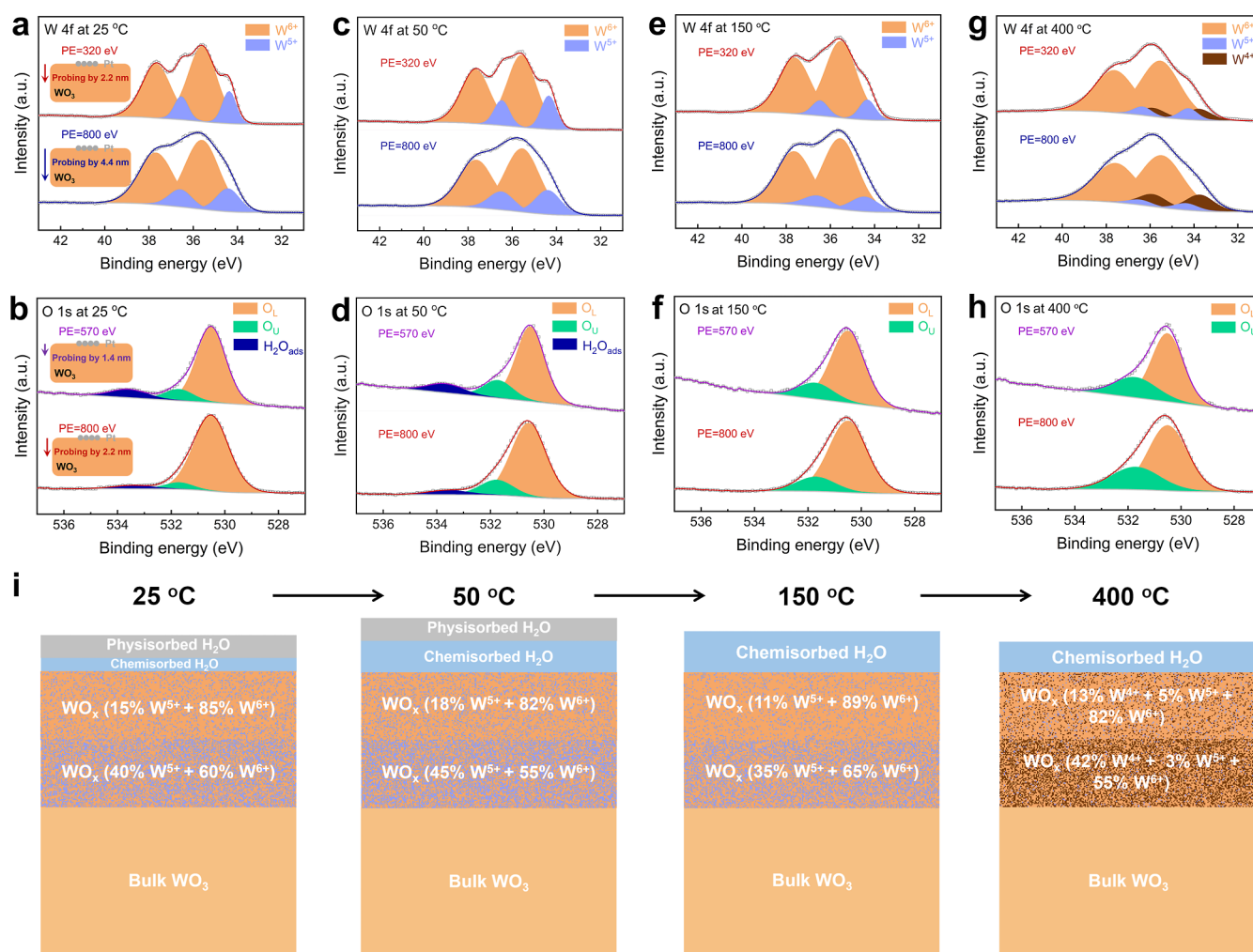


Figure 3. Depth profiles and models of Pt/WO₃ showing component variations at different temperatures. W 4f regions measured at 320 and 800 eV of photon energies in (a,c,e) and (g); O 1s regions measured at 570 and 800 eV of photon energies in (b,d,f,h), showing the chemical states of W and O on the surface of Pt/WO₃ at 25, 50, 150, and 400 °C, respectively. (i) SESSA modeling represents surface composition of Pt/WO₃ at 25, 50, 150, and 400 °C, indicating the ratios of W⁶⁺, W⁵⁺ and W⁴⁺ in the WO_x layers using checkerboard patterns with building squares in the same colors for the W species as those in (g).

cally favorable with a reaction energy of -1.02 eV at 25 °C. The activation energy barrier is calculated to be 0.29 eV. The second hydrogen atom spills over to the same terminal oxygen, with exergonic reaction energy of -0.21 eV and a higher activation energy barrier of 0.76 eV, indicating that the formation of H₂O_{ads} is the rate-determining step. At 25 °C, the formation of O_{vac} via H₂O_{ads} desorption is endergonic ($\Delta G = 0.22$ eV). On the contrary, H₂O_{ads} desorption becomes thermodynamically favored as the temperature is increased ($\Delta G = -0.64$ eV at 400 °C). Thus, the formation of O_{vac} becomes predominant at elevated temperatures. Microkinetic modeling (MKM) was further conducted to understand how the reaction temperature affects the steady-state surface coverage of various species on the Pt/WO₃ (001) surface (Figure S9). Table S2 reports the thermodynamic and kinetic parameters of the elementary steps in hydrogen spillover reaction network on Pt/WO₃. At 25 °C, the most dominant species are surface H₂O_{ads}. With increasing temperature, molecular H₂O_{ads} species start to desorb while leaving behind O_{vac}, until steady-state coverage of O_{vac} reaches a plateau at 150 °C, while the existing amount of $-OH$ species remains negligible invariably. These MKM and Gibbs free energy

results suggest the variable assignments of O_U peaks in the O 1s spectra at different temperatures. At room temperature, O_U species could represent chemisorbed H₂O. With increasing reaction temperature, H₂O_{ads} desorbs from the surface and thus O_{vac} gradually accumulates on the surface. Therefore, at elevated temperatures, O_U species could represent the integration of chemisorbed H₂O and O atoms near O_{vac}. These important computational findings inspired us to further experimentally explore the behaviors of the interfaces via a temperature-dependent APXPS strategy.

Further temperature-dependent APXPS measurements were used to assess these theoretical studies. A bare WO₃ sample was heated from room temperature to 400 °C in 7 steps under 5 mTorr of H₂. At each temperature, the sample was equilibrated while the W 4f and O 1s regions were continuously recorded for 30 min, which was sufficient to obtain stable spectra in each case. High-resolution W 4f and O 1s spectra were then measured with PEs of 320 and 800 eV, respectively (Figure S10), ensuring comparable probing depth (2.2 nm) for both elements in the sample. The results show negligible changes in the chemical states of W and O across the entire temperature range up to 400 °C, indicating that bare

WO₃ remained stable in the presence of H₂ at elevated temperatures. Introducing Pt metal clusters into WO₃ resulted in remarkably different interfacial dynamics, which also varied considerably with temperature. These changes were further measured by altering the PE to obtain depth profiles (Figures S11, S12 and Tables S3, S4). At each temperature, the PEs of 320 and 800 eV (probing depths of 2.2 and 4.4 nm, respectively) were chosen to investigate the W states, while the PEs of 570 and 800 eV (probing depths of 1.4 and 2.2 nm, respectively) were used to study the O states based on the photon flux distribution at the beamline.⁴¹ Upon equilibration under 5 mTorr H₂ at room temperature, W was found as a mixture of W⁵⁺ and W⁶⁺ on Pt/WO₃, with considerable amounts of O_U and H₂O_{ads} (Figure 3a,b), aligning with our aforementioned dynamic observations (Figure 2d,e). When the temperature increased from 25 to 50 °C, the amount of W⁵⁺ increased to its highest level within the entire temperature range, while the quantity of W⁶⁺ decreased correspondingly (Figures 3c,d and S11). Concurrently, increased quantities of O_U and H₂O_{ads} were also observed. We interpret these observations as evidence of hydrogen dissociation and spillover, resulting in W reduction and the accumulation of hydrogen intermediates on the surface of Pt/WO₃ via PCET. Based on the depth profiles (Figure S11), a slightly larger quantity of W⁵⁺ was found deeper in the lattice (4.4 nm depth) compared to the subsurface (2.2 nm), implying the facile transport of spillover H atoms into the oxide lattice besides the formation of H₂O_{ads} and slightly higher stability for the species in the bulk versus surface sites.^{17,28,39} This migration behavior of hydrogen helps mitigate hydrogen poisoning, especially minimizing the negative impact on surface sites. High mobility of protons in the monoclinic WO₃ lattice²¹ also supports the feasibility to avoid the hydrogen poisoning effect. Furthermore, the presence of H₂O_{ads} catalytically facilitates hydrogen migration by bridging two separated oxygen atoms, transporting hydrogen from the WO₃ top surface layer to subsurface layers, reducing hydrogen poisoning.⁴⁰

When the temperature increased further from 50 °C, dissociated hydrogen atoms spilled over to both surface and bulk. On the surface, H₂O_{ads} molecules started to desorb to the gas phase, leaving behind abundant O_{vac} sites.^{12,15,20} At elevated temperatures, O_U species can be interpreted as the integration of chemisorbed H₂O and O atoms near O_{vac} species. The H₂O_{ads} signal at 533.8 eV disappears at 100 °C, which can be regarded as an indication that H₂O_{ads} evaporates, implying the assignment of this H₂O_{ads} peak in O 1s region to physisorbed H₂O (Figure S12).^{37,38} In the bulk, hydrogen atoms diffused inward binding with O_L,¹⁷ leading to reduction of the near W site. As a result, the amount of subsurface W⁶⁺ (penetrating to 2.2 nm) was higher than that in deeper depth (4.4 nm) (Figure S11). Notably, hydrogenated H_xWO₃ serves as an efficient proton conductor, exhibiting barrierless proton mobility within its bulk.^{21,40} However, the formation of molecular H₂ in the bulk of H_xWO₃ is kinetically hindered, with an energy barrier of 2.25 eV on H_{0.5}WO₃.²¹ In contrast, H₂ formation on the surface of WO₃ is kinetically more favorable (Figure 1). Consequently, it is challenging to entirely exclude the possibility of reverse H₂ formation on the surface of H_xWO₃, especially given the facile diffusion of lattice protons from the bulk to the surface.²¹ On the other hand, H₂ formation on Pt clusters faces a significant kinetic trap due to the strong binding of dissociated hydrogen atoms to Pt clusters (Figure 1), suggesting that reverse H₂ formation on Pt clusters

is unlikely. From 50 to 150 °C, the average oxidation state of W atoms increased as the amount of W⁶⁺ and O_L kept rising, which reached maximum at 150 °C (Figures 3c–f, S11 and S12). There are two ways where this reoxidation phenomenon can occur: (I) H* species diffuse from surface to bulk sites (not probed by XPS) and bind with O_L to form H_xWO₃; (II) H* species on the surface of WO₃ undergo reverse hydrogen spillover facilitated by H_xWO₃, with the formation of H₂ molecules on Pt metal followed by the desorption of H₂ to the gas phase.⁴² Based on the gradient reduced W species from the surface to bulk (Figure S11), the inward migration of H* happened over the whole range of temperature. Meanwhile, heating likely drives reverse spillover of H* species to regenerate gas-phase H₂ molecules^{22,23} based on the entropic contributions at elevated temperatures. It was also reported that reverse hydrogen spillover from WO₃ to Pt₆ cluster was feasible.⁴⁰ However, it is challenging to differentiate the superior pathway between surface-to-bulk diffusion and reverse spillover of H* species based on current characterization techniques. We propose that both possible pathways surpass surface spillover of H* species and thus cause surface reoxidation in the temperature range of 50–150 °C.

As the temperature increased beyond 150 °C, H₂O_{ads} desorption was further facilitated, making surface spillover predominant. Consequently, W⁴⁺ was detected, and a large quantity of O_{vac} sites formed, as indicated by much more deconvoluted O_U species (Figures 3g,h, S11 and S12). As the inward hydrogen diffusion still occurred and was even enhanced compared to that at lower temperatures, incremental gradients of reduced W (W⁴⁺ and W⁵⁺) and O_U were observed from the surface to the bulk (Figures S11 and S12). In the temperature range of 150–400 °C, with the marginally superior H₂O_{ads} desorption, W was continuously reduced and O_{vac} sites accumulated on the WO₃ substrate as a result of oxygen loss and the formation of substoichiometric WO_x phases.^{20,43} Throughout this process, Pt metal clusters showed negligible changes, scarcely affecting the H₂ activation (Figure S13).

To better understand the dynamic evolution in the APXPS experiments, we further simulated the surface components of Pt/WO₃ at 25, 50, 150, and 400 °C using the SESSA software package^{44,45} based on the experimental fractions of W and O species. The validation of the models for elucidating surface evolution at variable temperatures is proved by the highly comparable fractions of W and O species between experiments and modeling (Figure 3i and Table S5). At room temperature, there are two layers of tungsten oxide (WO_x) above the bulk WO₃, showing more reduced W species at greater depth, where W was partially reduced to W⁵⁺. Above the two layers of WO_x, there are two layers of H₂O_{ads} as the products of surface hydrogen spillover. One is due to chemisorption with strong binding between H₂O and WO_x; the other is generated by weak binding of H₂O on WO_x as a result of desorption of H₂O from a chemisorbed state. As the temperature reaches 50 °C, the amount of W⁵⁺ and chemisorbed H₂O further increases, indicating hydrogen dissociation and spillover on the surface are enhanced. At 150 °C, H₂O_{ads} with weak binding on WO_x desorbs to the gas phase, and the chemisorbed H₂O with strong binding on WO_x becomes thicker. An increasing ratio of W⁶⁺/W⁵⁺ in the two surface layers of WO_x indicates the surface reoxidation led by surface-to-bulk diffusion and reverse spillover of H* species. When it comes to 400 °C, H₂O_{ads} desorption is significantly facilitated, resulting in the formation

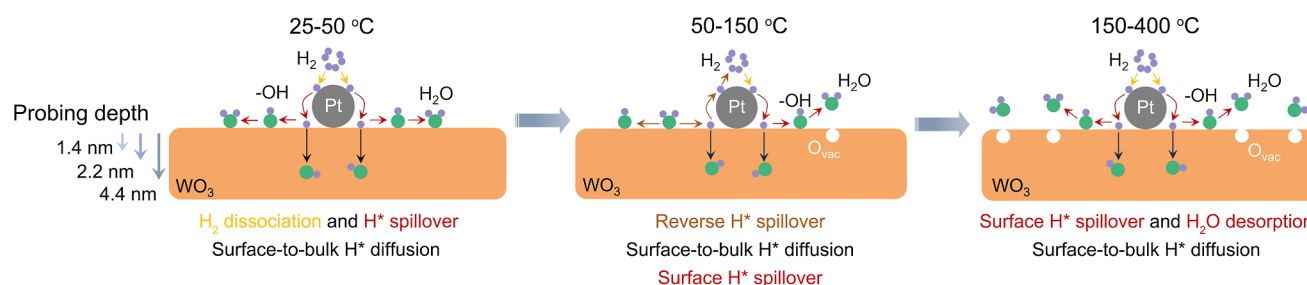


Figure 4. Schematic illustration of the reaction mechanisms at varied temperatures. Orange rectangle represents the crystalline WO₃ substrate. Solid green, purple, gray and white balls stand for O, H, Pt elements and O_{vac} sites, respectively.

of W⁴⁺ in the WO_x layers. Concurrently, surface-to-bulk diffusion of hydrogen atoms continues to drive an increasing concentration of reduced W species with increasing depth (Figure S14 and Table S5). These models make the surface states of the substrate more visible and provide a clear understanding of reaction mechanisms at different temperatures.

To summarize, the three predominant reaction processes at each of three corresponding temperature ranges are schematically depicted in Figure 4. H₂ molecules dissociate, spill over, and interact with monoclinic WO₃ at different temperatures induced by Pt metal, leading to dynamic changes in W and O states (Figure S15), which were revealed by *operando* soft X-ray APXPS combined with DFT calculations and microkinetic modeling.

CONCLUSIONS

In summary, this work investigates Pt-induced hydrogen interaction with WO₃ by *operando* APXPS in combination with first-principles-based multiscale modeling. It reveals the key role of Pt metal clusters in facilitating the activation and dissociation of H₂ molecules, as well as the subsequent spillover of hydrogen atoms onto the WO₃ surface. The dynamic evolution of surface states was further elucidated through time- and temperature-dependent APXPS experiments and SESSA simulations. At room temperature, hydrogen spillover contributes to W reduction toward W⁵⁺ and the formation of hydrogen intermediates (–OH and H₂O_{ads}) via PCET. In the temperature range of 50–150 °C, surface-to-bulk diffusion and reverse spillover of hydrogen atoms were enhanced compared to surface spillover, which resulted in surface reoxidation. When the temperature reached beyond 150 °C, H₂O_{ads} desorption took over, leading to dynamic reduction of W species and accumulation of O_{vac} sites on the WO₃ surface. These findings, supported by experimental observations using APXPS, first-principles-based microkinetic modeling, and SESSA simulations, provide a comprehensive understanding of the reaction mechanisms underlying hydrogen spillover on reducible metal oxides, offering valuable insights into the control of catalytic hydrogen-related transformations.

ASSOCIATED CONTENT

Supporting Information

The Supporting Information is available free of charge at <https://pubs.acs.org/doi/10.1021/jacs.4c13711>.

Cartesian coordinates of relevant DFT structures (TXT)
Detailed preparation methods of samples, APXPS experimental methods, DFT calculations, microkinetic

modeling and additional data were shown to support our conclusions (PDF)

AUTHOR INFORMATION

Corresponding Authors

Giannis Mpourmpakis – Department of Chemical and Petroleum Engineering, University of Pittsburgh, Pittsburgh, Pennsylvania 15261, United States; School of Chemical Engineering, National Technical University of Athens, Athens GR-15780, Greece; orcid.org/0000-0002-3063-0607; Email: GMPOURMP@pitt.edu

Ethan J. Crumlin – Chemical Sciences Division, Lawrence Berkeley National Laboratory, Berkeley, California 94720, United States; Advanced Light Source, Lawrence Berkeley National Laboratory, Berkeley, California 94720, United States; orcid.org/0000-0003-3132-190X; Email: ejcrumlin@lbl.gov

Authors

Haoyi Li – Chemical Sciences Division, Lawrence Berkeley National Laboratory, Berkeley, California 94720, United States; orcid.org/0000-0002-0723-8068

Mona Abdelgaid – Department of Chemical and Petroleum Engineering, University of Pittsburgh, Pittsburgh, Pennsylvania 15261, United States; orcid.org/0000-0003-0973-3262

Jay R. Paudel – Chemical Sciences Division, Lawrence Berkeley National Laboratory, Berkeley, California 94720, United States; orcid.org/0000-0002-3173-3018

Noah P. Holzapfel – Department of Materials Science and Engineering, North Carolina State University, Raleigh, North Carolina 27606, United States; orcid.org/0000-0002-4566-4033

Veronica Augustyn – Department of Materials Science and Engineering, North Carolina State University, Raleigh, North Carolina 27606, United States; orcid.org/0000-0001-9885-2882

James R. McKone – Department of Chemical and Petroleum Engineering, University of Pittsburgh, Pittsburgh, Pennsylvania 15261, United States; Department of Chemistry, University of Pittsburgh, Pittsburgh, Pennsylvania 15261, United States; orcid.org/0000-0001-6445-7884

Complete contact information is available at: <https://pubs.acs.org/doi/10.1021/jacs.4c13711>

Author Contributions

H.L. and M.A. contributed equally to this work.

Notes

The authors declare no competing financial interest.

ACKNOWLEDGMENTS

This manuscript is based on work supported by the U.S. Department of Energy, Office of Science, Office of Basic Energy Sciences, under contract no. DE-SC0023465. E.J.C. was partially supported by the Condensed Phase and Interfacial Molecular Science Program (CPIMS) of the U.S. Department of Energy under contract no. DE-AC02-0511231. G.M. and M.A. acknowledge computational support from the Center for Research Computing at the University of Pittsburgh, RRID: SCR_022735, through the resources provided. Specifically, this work used the H2P cluster, which is supported by NSF award no. OAC-2117681.

REFERENCES

- (1) Keijer, T.; Bakker, V.; Slootweg, J. C. Circular chemistry to enable a circular economy. *Nat. Chem.* **2019**, *11* (3), 190–195.
- (2) Kümmerer, K.; Clark, J. H.; Zuin, V. G. Rethinking chemistry for a circular economy. *Science* **2020**, *367* (6476), 369–370.
- (3) Li, H.; Chen, S.; Zhang, Y.; Zhang, Q.; Jia, X.; Zhang, Q.; Gu, L.; Sun, X.; Song, L.; Wang, X. Systematic design of superaerophobic nanotube-array electrode comprised of transition-metal sulfides for overall water splitting. *Nat. Commun.* **2018**, *9* (1), 2452.
- (4) Lu, Z.; Cooney, S. E.; McKone, J. R.; Matson, E. M. Selective Hydrogenation of Azobenzene to Hydrazobenzene via Proton-Coupled Electron Transfer from a Polyoxotungstate Cluster. *JACS Au* **2024**, *4* (4), 1310–1314.
- (5) Zaera, F. The Surface Chemistry of Metal-Based Hydrogenation Catalysis. *ACS Catal.* **2017**, *7* (8), 4947–4967.
- (6) Zhang, L.; Zhou, M.; Wang, A.; Zhang, T. Selective Hydrogenation over Supported Metal Catalysts: From Nanoparticles to Single Atoms. *Chem. Rev.* **2020**, *120* (2), 683–733.
- (7) Conner, W. C.; Falconer, J. L. Spillover in heterogeneous catalysis. *Chem. Rev.* **1995**, *95* (3), 759–788.
- (8) Prins, R. Hydrogen Spillover. Facts and Fiction. *Chem. Rev.* **2012**, *112* (5), 2714–2738.
- (9) Fouad, N. E. Impacts of hydrogen spillover on the reduction behavior of tungsten oxide: Isothermal and non-isothermal approaches. *J. Anal. Appl. Pyrolysis* **1997**, *44* (1), 13–28.
- (10) Benson, J. E.; Kohn, H. W.; Boudart, M. On the reduction of tungsten trioxide accelerated by platinum and water. *J. Catal.* **1966**, *5* (2), 307–313.
- (11) Koverga, A. A.; Flórez, E.; Jimenez-Orozco, C.; Rodriguez, J. A. Spot the difference: hydrogen adsorption and dissociation on unsupported platinum and platinum-coated transition metal carbides. *Phys. Chem. Chem. Phys.* **2021**, *23* (36), 20255–20267.
- (12) Beck, A.; Kazazis, D.; Ekinci, Y.; Li, X.; Müller Gubler, E. A.; Kleibert, A.; Willinger, M.-G.; Artiglia, L.; van Bokhoven, J. A. The Extent of Platinum-Induced Hydrogen Spillover on Cerium Dioxide. *ACS Nano* **2023**, *17* (2), 1091–1099.
- (13) Chen, J.-W.; Hsieh, S.-H.; Wong, S.-S.; Chiu, Y.-C.; Shiu, H.-W.; Wang, C.-H.; Yang, Y.-W.; Hsu, Y.-J.; Convertino, D.; Coletti, C.; Heun, S.; Chen, C.-H.; Wu, C.-L. Hydrogen Spillover and Storage on Graphene with Single-Site Ti Catalysts. *ACS Energy Lett.* **2022**, *7* (7), 2297–2303.
- (14) Mehar, V.; Huang, E.; Shi, R.; Rui, N.; Rosales, R.; Waluyo, I.; Hunt, A.; Liu, P.; Rodriguez, J. A. Microscopic Investigation of H₂ Reduced CuO_x/Cu(111) and ZnO/CuO_x/Cu(111) Inverse Catalysts: STM, AP-XPS, and DFT Studies. *ACS Catal.* **2023**, *13* (14), 9857–9870.
- (15) Yoon, H.; Kim, Y.; Crumlin, E. J.; Lee, D.; Ihm, K.; Son, J. Direct Probing of Oxygen Loss from the Surface Lattice of Correlated Oxides during Hydrogen Spillover. *J. Phys. Chem. Lett.* **2019**, *10* (22), 7285–7292.
- (16) Huynh, M. H. V.; Meyer, T. J. Proton-Coupled Electron Transfer. *Chem. Rev.* **2007**, *107* (11), 5004–5064.
- (17) Miu, E. V.; McKone, J. R.; Mpourmpakis, G. The Sensitivity of Metal Oxide Electrocatalysis to Bulk Hydrogen Intercalation: Hydrogen Evolution on Tungsten Oxide. *J. Am. Chem. Soc.* **2022**, *144* (14), 6420–6433.
- (18) Spencer, M. A.; Fortunato, J.; Augustyn, V. Electrochemical proton insertion modulates the hydrogen evolution reaction on tungsten oxides. *J. Chem. Phys.* **2022**, *156* (6), 064704.
- (19) Cheng, H.; Chen, L.; Cooper, A. C.; Sha, X.; Pez, G. P. Hydrogen spillover in the context of hydrogen storage using solid-state materials. *Energy Environ. Sci.* **2008**, *1* (3), 338–354.
- (20) Shun, K.; Mori, K.; Masuda, S.; Hashimoto, N.; Hinuma, Y.; Kobayashi, H.; Yamashita, H. Revealing hydrogen spillover pathways in reducible metal oxides. *Chem. Sci.* **2022**, *13* (27), 8137–8147.
- (21) Spencer, M. A.; Holzapfel, N. P.; You, K.-E.; Mpourmpakis, G.; Augustyn, V. Participation of electrochemically inserted protons in the hydrogen evolution reaction on tungsten oxides. *Chem. Sci.* **2024**, *15* (14), 5385–5402.
- (22) Chen, J.; Chen, C.; Qin, M.; Li, B.; Lin, B.; Mao, Q.; Yang, H.; Liu, B.; Wang, Y. Reversible hydrogen spillover in Ru-WO_{3-x} enhances hydrogen evolution activity in neutral pH water splitting. *Nat. Commun.* **2022**, *13* (1), 5382.
- (23) Gao, Z.; Wang, G.; Lei, T.; Lv, Z.; Xiong, M.; Wang, L.; Xing, S.; Ma, J.; Jiang, Z.; Qin, Y. Enhanced hydrogen generation by reverse spillover effects over bicomponent catalysts. *Nat. Commun.* **2022**, *13* (1), 118.
- (24) Jenkinson, K.; Spadaro, M. C.; Golovanova, V.; Andreu, T.; Morante, J. R.; Arbiol, J.; Bals, S. Direct Operando Visualization of Metal Support Interactions Induced by Hydrogen Spillover During CO₂ Hydrogenation. *Adv. Mater.* **2023**, *35* (51), 2306447.
- (25) Lee, J.; Tieu, P.; Finzel, J.; Zang, W.; Yan, X.; Graham, G.; Pan, X.; Christopher, P. How Pt Influences H₂ Reactions on High Surface-Area Pt/CeO₂ Powder Catalyst Surfaces. *JACS Au* **2023**, *3* (8), 2299–2313.
- (26) Wei, J.; Qin, S.-N.; Liu, J.-L.; Ruan, X.-Y.; Guan, Z.; Yan, H.; Wei, D.-Y.; Zhang, H.; Cheng, J.; Xu, H.; Tian, Z.-Q.; Li, J.-F. In Situ Raman Monitoring and Manipulating of Interfacial Hydrogen Spillover by Precise Fabrication of Au/TiO₂/Pt Sandwich Structures. *Angew. Chem., Int. Ed.* **2020**, *59* (26), 10343–10347.
- (27) Kavre Piltaver, I.; Peter, R.; Salamon, K.; Micetic, M.; Petravic, M. In Situ X-ray Photoelectron Spectroscopy Study of Initial Stages of Tungsten Trioxide Reduction by Low-Energy Hydrogen Bombardment. *J. Phys. Chem. C* **2024**, *128* (12), 5345–5354.
- (28) Miu, E. V.; Mpourmpakis, G.; McKone, J. R. Predicting the Energetics of Hydrogen Intercalation in Metal Oxides Using Acid–Base Properties. *ACS Appl. Mater. Interfaces* **2020**, *12* (40), 44658–44670.
- (29) Zhou, C.; Wu, J.; Nie, A.; Forrey, R. C.; Tachibana, A.; Cheng, H. On the Sequential Hydrogen Dissociative Chemisorption on Small Platinum Clusters: A Density Functional Theory Study. *J. Phys. Chem. C* **2007**, *111* (34), 12773–12778.
- (30) Aireddy, D. R.; Ding, K. Heterolytic Dissociation of H₂ in Heterogeneous Catalysis. *ACS Catal.* **2022**, *12* (8), 4707–4723.
- (31) Jing, Y.; Wang, Y. Heterolytic dissociation of H₂ and bond activation: Spotting new opportunities from a unified view. *Chem Catal.* **2023**, *3* (3), 100515.
- (32) Mitchell, J. B.; Lo, W. C.; Genc, A.; LeBeau, J.; Augustyn, V. Transition from Battery to Pseudocapacitor Behavior via Structural Water in Tungsten Oxide. *Chem. Mater.* **2017**, *29* (9), 3928–3937.
- (33) Petzoldt, P.; Eder, M.; Mackewicz, S.; Blum, M.; Kratky, T.; Günther, S.; Tschurl, M.; Heiz, U.; Lechner, B. A. J. Tuning Strong Metal–Support Interaction Kinetics on Pt-Loaded TiO₂(110) by Choosing the Pressure: A Combined Ultrahigh Vacuum/Near-Ambient Pressure XPS Study. *J. Phys. Chem. C* **2022**, *126* (38), 16127–16139.
- (34) Rieboldt, F.; Helveg, S.; Bechstein, R.; Lammich, L.; Besenbacher, F.; Lauritsen, J. V.; Wendt, S. Formation and sintering of Pt nanoparticles on vicinal rutile TiO₂ surfaces. *Phys. Chem. Chem. Phys.* **2014**, *16* (39), 21289–21299.
- (35) Rieboldt, F.; Vilhelmsen, L. B.; Koust, S.; Lauritsen, J. V.; Helveg, S.; Lammich, L.; Besenbacher, F.; Hammer, B.; Wendt, S.

Nucleation and growth of Pt nanoparticles on reduced and oxidized rutile TiO₂ (110). *J. Chem. Phys.* **2014**, *141* (21), 214702.

(36) Braun, A.; Aksoy Akgul, F.; Chen, Q.; Erat, S.; Huang, T.-W.; Jabeen, N.; Liu, Z.; Mun, B. S.; Mao, S. S.; Zhang, X. Observation of Substrate Orientation-Dependent Oxygen Defect Filling in Thin WO_{3-δ}/TiO₂ Pulsed Laser-Deposited Films with in Situ XPS at High Oxygen Pressure and Temperature. *Chem. Mater.* **2012**, *24* (17), 3473–3480.

(37) Frankcombe, T. J.; Liu, Y. Interpretation of Oxygen 1s X-ray Photoelectron Spectroscopy of ZnO. *Chem. Mater.* **2023**, *35* (14), 5468–5474.

(38) Shpak, A. P.; Korduban, A. M.; Medvedskij, M. M.; Kandyba, V. O. XPS studies of active elements surface of gas sensors based on WO_{3-x} nanoparticles. *J. Electron. Spectrosc.* **2007**, *156–158*, 172–175.

(39) Miu, E. V.; McKone, J. R. Comparisons of WO₃ reduction to H_xWO₃ under thermochemical and electrochemical control. *J. Mater. Chem. A* **2019**, *7* (41), 23756–23761.

(40) Xi, Y.; Zhang, Q.; Cheng, H. Mechanism of Hydrogen Spillover on WO₃(001) and Formation of H_xWO₃ ($x = 0.125, 0.25, 0.375, \text{ and } 0.5$). *J. Phys. Chem. C* **2014**, *118* (1), 494–501.

(41) Cai, J.; Han, Y.; Chen, S.; Crumlin, E. J.; Yang, B.; Li, Y.; Liu, Z. CO₂ Activation on Ni(111) and Ni(100) Surfaces in the Presence of H₂O: An Ambient-Pressure X-ray Photoelectron Spectroscopy Study. *J. Phys. Chem. C* **2019**, *123* (19), 12176–12182.

(42) Xie, C.; Chen, W.; Du, S.; Yan, D.; Zhang, Y.; Chen, J.; Liu, B.; Wang, S. In-situ phase transition of WO₃ boosting electron and hydrogen transfer for enhancing hydrogen evolution on Pt. *Nano Energy* **2020**, *71*, 104653.

(43) Lee, Y.-J.; Lee, T.; Soon, A. Phase Stability Diagrams of Group 6 Magnéli Oxides and Their Implications for Photon-Assisted Applications. *Chem. Mater.* **2019**, *31* (11), 4282–4290.

(44) Machida, A.; Nagata, K.; Murakami, R.; Shinotsuka, H.; Shouno, H.; Yoshikawa, H.; Okada, M. Bayesian inference method utilizing SESSA in quantitative layer structure estimation from XPS data. *J. Electron Spectrosc.* **2024**, *273*, 147449.

(45) Smekal, W.; Werner, W. S. M.; Powell, C. J. Simulation of electron spectra for surface analysis (SESSA): a novel software tool for quantitative Auger-electron spectroscopy and X-ray photoelectron spectroscopy. *Surf. Interface Anal.* **2005**, *37* (11), 1059–1067.